J. Condensed Matter Nucl. Sci. 24 (2017) 98–113

Research Article

Developing Phonon–Nuclear Coupling Experiments with Vibrating Plates and Radiation Detectors

Florian Metzler, Peter L. Hagelstein* and Siyuan Lu

Massachusetts Institute of Technology, Cambridge, MA, USA

Abstract

Excess heat has been reported in cold fusion experiments since 1989; however, there is at present no accepted explanation for what mechanisms are involved. Over the past decades a general theory has been developed which seems applicable to excess heat and other anomalies systematically; but in this case we do not yet have unambiguous experimental support for the phonon–nuclear coupling and enhanced up-conversion and down-conversion mechanism. This has motivated experimental studies with which we hope to develop relevant experimental results from which clear tests of theory can be made. A facility has been developed with which we are able to induce vibrations in metal plates from about 10 kHz up to about 10 MHz and then measure the relative displacement. With a high-power piezo transducer we have driven a steel plate at 2.23 MHz to produce a vibrational power of 100 W. We are able to detect X-rays with film, scintillator and camera, with low-cost sensitive scintillator/PMT detectors, and with an Amptek X-123 detector. We also have detectors that can see gamma and neutron emission.
 ISSN 2227-3123

Keywords: Karabut experiment, kHz and MHz transducers, Phonon–nuclear coupling, Radiation detection, Up-conversion

1. Introduction

Following the announcement of excess heat in the Fleischmann–Pons experiment [1,2] there have been a large number of studies performed within our community seeking excess heat in PdD in electrochemical and in gas loading experiments [3]. Correlations between excess heat and current density, loading, temperature, ^{4}He, RF emission, neutron emission and gamma emission have all been pursued; as well as tests for excess heat with Pd alloys and with other metals; and also with hydrogen and mixed H/D loading. A presumption implicit in this research is that by understanding more about the system we might come closer to understanding how it works microscopically. Due to the large amount of energy produced, and absence of commensurate chemical products, the origin of the energy must be nuclear. When nuclear energy is created in conventional nuclear fission or fusion reactions, energetic particles are observed in amounts commensurate with the energy; in this case we are able to understand how the microscopic reactions work by detecting the energetic particles and comparing with theoretical predictions from nuclear physics. In

*E-mail: plh@mit.edu

 ISSN 2227-3123

the Fleischmann–Pons experiment the absence of commensurate energetic particles then prevents us from making use of standard nuclear methods to study microscopic mechanisms, with the result that after almost 28 years there remains no agreement as to what mechanism is responsible for the excess heat effect. This has hindered scientific progress, and has made it difficult to interact with skeptical colleagues who are not convinced that there is a real effect worthy of study.

Basic physics issues associated with the excess heat effect have been considered in our group for many years. The absence of commensurate energetic particles in connection with excess heat production has been identified as the most fundamental of the theoretical issues, which for us implies the existence of a mechanism capable of down-conversion from the MeV regime down to an energy scale relevant to condensed matter energy scales at the eV level or below [4]. In 2002 a relatively simple mechanism was proposed that could lead to a strongly enhanced down-conversion effect that appears to be sufficiently strong to be relevant to the problem. Subsequently an interaction mechanism was identified in which internal degrees of freedom of a nucleus is coupled to the center of mass motion [5]. This coupling, combined with the down-conversion mechanism, can provide a foundation for a theoretical description of the excess heat effect, as well as other anomalies. Continued progress on the models provides encouragement that an acceptable theoretical solution will emerge; however, a connection between the emerging theory and experiment is needed. For example, if there really is a coupling between internal nuclear degrees of freedom and vibrations, then there should be observable consequences independent of the Fleischmann–Pons experiment. If a large quantum can be down-converted, then this or the inverse up-conversion effect should be observable, again independent of the Fleischmann–Pons experiment.

These considerations have in part provided motivation for an experimental effort focused on providing experimental feedback in response to the theoretical ideas that have been put forth. There are a number of experiments which have been reported previously in which interpretations involving up-conversion are possible; these include collimated X-ray emission in the Karabut experiment [6]; collimated X-ray emission in the waterjet experiments of Kornilova and coworkers [7]; neutron emission from a steel sample that is vibrated in the experiments of Cardone and coworkers [8]; and fracture experiments of Carpinteri and coworkers [9] where neutron emission and other effects are reported when large granite samples containing iron are fractured. We are interested in whether unambiguous experimental evidence for phonon–nuclear coupling can be developed, and whether a case can be made for up-conversion or down-conversion in the phonon–nuclear coupled system.

2. Input from Theory

Models based on the lossy spin–boson system describe up-conversion and down-conversion as being essentially the same theoretically, so that we expect to understand the down-conversion mechanism from experiments involving up-conversion. In this model a highly excited oscillator is linearly coupled with many identical two-level systems in the presence of loss. In order for the up-conversion of many oscillator quanta to create a single two-level excitation to occur within the model with a significant rate, the coupling must be sufficiently strong so that [10]

$$(\hbar\omega_0)^3 V_0 \left\langle \sqrt{S^2 - m^2}\sqrt{n} \right\rangle \; > \; 2 \times 10^{-4} \Delta E^4, \tag{1}$$

where $\hbar\omega_0$ is the phonon energy, V_0 the coupling strength, n the number of phonons in the mode, ΔE the excitation energy, and $\sqrt{S^2 - m^2}$ is the Dicke number. This constraint has the best chance to be satisfied when the (nuclear) excitation energy ΔE is minimized, when the (vibrational phonon) oscillator energy $\hbar\omega_0$ is maximized, when n is large so that the (phonon) mode is highly excited, and when the Dicke number is large which means that many nuclei are involved.

These considerations suggest that our focus should be on low energy nuclear transitions (to have a small ΔE), some of which are listed in Table 1, high frequency vibrational modes, strong vibrational excitation, and large samples.

Table 1. Some important low-energy nuclear transitions [7].

Isotope	Natural abundance (%)	Energy (keV)	Half-life	Multipolarity
Hg-201	13.2	1.565	81 ns	M1+E2
Ta-181	100	6.237	6.05 μs	E1
Fe-57	2.1	14.4129	98.3 ns	M1+E2

The phonon–nuclear interaction that arises from a relativistic model has E1 multipolarity, which suggests that the 6.237 keV transition in ^{181}Ta is particularly interesting to us. M1 transitions are possible with two-phonon exchange, but we would expect them to be weaker. The 1.565 keV transition is also very interesting since it is the lowest energy transition from the ground state of all the stable nuclei. We note that collimated X-ray emission in the Karabut experiment is reported near 1.5 keV [6], which is compatible with an interpretation of this experiment as demonstrating up-conversion of vibrations to produce phase-coherent excitation of this transition in ^{201}Hg nuclei as an impurity near the cathode surface. The cathode is mechanically coupled to a cathode support and large stainless steel vacuum chamber, which is of interest here in that inadvertently a large number of ^{57}Fe nuclei can share common vibrations in the system. Perhaps up-conversion of vibrations occurs due to the 14.4 keV transition in the vacuum chamber, with the excitation transferred to produce excitation in the ^{201}Hg nuclei below the cathode surface resulting ultimately in collimated X-ray emission. In order for a highly-excited oscillator strongly coupled to many two-level systems at energy ΔE_1 in the presence of loss to up-convert to two-level systems at a lower energy ΔE_2, we expect conversion to be hindered unless [12]

$$\frac{(\hbar\omega_0)^3 V_0 \left\langle \sqrt{S^2 - m^2}\sqrt{n} \right\rangle}{(\Delta E_1)^3} > 2 \times 10^{-4} \Delta E_2. \tag{2}$$

Earlier efforts to apply the up-conversion model to calculate up-conversion of vibrations in the MHz range to produce excitation in the keV regime were basically unsuccessful. However, we have recently understood that the models are compatible with up-conversion in stages, where instead of up-converting from MHz frequencies to produce excitation in the keV regime in a single step, the numbers work much better if the up-conversion involves intermediate steps. In this case up-conversion of a strongly excited oscillator at ω_0 coupled with many two-level transitions at ΔE in the presence of loss would be expected to produce excitation in a vibrational mode at higher frequency ω_1 when

$$\frac{(\hbar\omega_0)^3 V_0 \left\langle \sqrt{S^2 - m^2}\sqrt{n} \right\rangle}{\Delta E^3} > 2 \times 10^{-4} \hbar\omega_1. \tag{3}$$

In this case we might imagine up-conversion from MHz vibrations to GHz vibrations; then a second step of up-conversion of GHz vibrations to THz vibrations; and finishing up with up-conversion to the keV regime. There are issues associated with momentum conservation in the coupling matrix elements since disparate wavelength are involved; however, this may still work out since ^{57}Fe is present at low levels (and hence is not present at every site).

Excitation transfer experiments seem possible as a way to test the proposed phonon–nuclear coupling, where excited state ^{181}Ta (or ^{57}Fe) nuclei are produced as a result of radioactive decay of ^{181}W (or ^{57}Co); where gamma emission from nuclei away from where the initial excitation is produced would signal that excitation transfer has occurred. If the proposed interpretation of up-conversion in the Karabut experiment is right, then perhaps it is possible to develop new experiments where (large) steel samples are vibrated and X-ray emission sought from a small amount of mercury added near the surface. As noted above we have conjectured that neutron emission and transmutation claimed in some of Cardone's experiments [8], where steel samples are vibrated very strongly at 20 kHz, may be

a result of up-conversion resulting in neutron emission [13]. We note reports from Carpinteri of the observation of neutron emission and elemental anomalies in fractured granite containing iron [9]. In recent experiments reported by Cardone and coworkers liquid mercury is vibrated very strongly resulting in apparent elemental and isotopic anomalies [14], which also permits an interpretation of up-conversion. If so, then perhaps we might be able to see anomalies in samples with low energy nuclear transitions that are vibrated strongly, and test whether the conjectures from theory are correct or not.

3. Experimental, Generation and Observation of Vibrations

In earlier experiments carried out at SRI and at MIT, capacitive coupling through air or PVDF (polyvinylidene fluoride) was used to stimulate vibrations in the range of 10–50 MHz, where the relatively high frequency range was chosen to maximize the phonon energy following the arguments above [15]. Due to the various technical difficulties encountered in this work, and in the initial MIT efforts, we decided to work at lower frequencies so that the experiments might be easier generally, and also to reduce issues with noise that plagued the earlier work.

3.1. Wide-band transducers and laser amplitude modulation

In our system sinusoidal signals originate in a computer controlled tunable signal generator; they can be amplified by a linear amp; and then the signal is coupled through a dual directional coupler to a transducer coupled to a metal plate (Fig. 1).

To detect the vibrational response we initially attempted to make use of FM modulation using a laser in a homodyne detection system; however, we found that the signals detected were due instead to amplitude modulation. When we first collected spectra in the MHz regime, a large number of resonances combined to produce a complicated spectrum.

For a rectangular plate the (unloaded) compressional resonances are at

$$f_{lmn} = \sqrt{\left(\frac{c_L l}{2L_x}\right)^2 + \left(\frac{c_L m}{2L_y}\right)^2 + \left(\frac{c_L n}{2L_z}\right)^2} \tag{4}$$

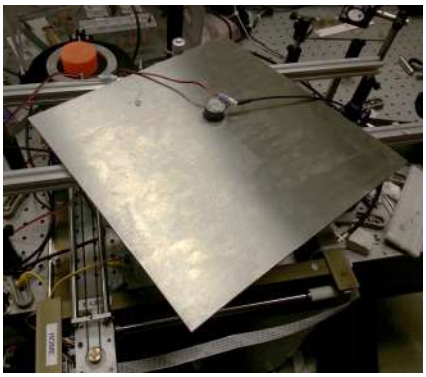

Figure 1. Steel plate 3 mm thick, $12'' \times 12''$ transverse dimensions with broadband transducer.

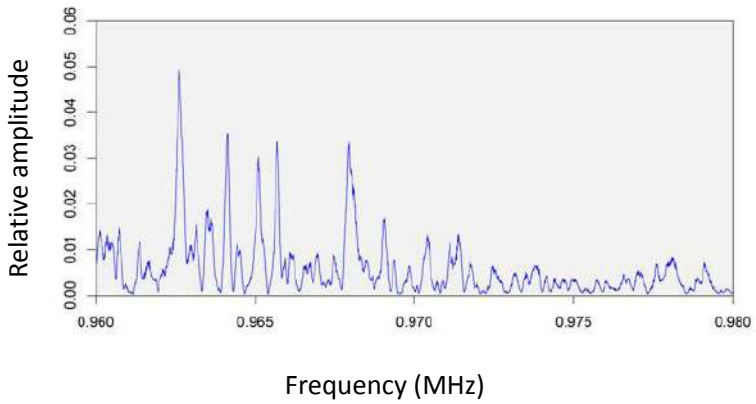

Figure 2. Compressional spectrum for the steel plate of Fig. 1 near the $n = 1$ fundamental.

where c_L is the compressional sound speed, where L_x, L_y and L_z are the plate dimensions in the three directions. We are most interested in the fundamental (where $l = m = 0, n = 1$) and the low harmonics ($n = 2, 3, \ldots$) since these are transversely uniform in the ideal case. In order to find the fundamental we tried working with a shallow incident laser beam, hoping for a stronger response from the fundamental and harmonics than from modes with transverse structure. This was helpful, but we still observed many lines in the vibrational spectrum as shown in Fig. 2. In this case we worked with a steel plate 3 mm thick, motivated by the 3 mm thick steel plates used by Kornilova and coworkers in their collimated X-ray experiments with a waterjet [7]. An example of a spectrum in the vicinity of the 3rd and 4th harmonic of the compressional fundamental of a 3 mm Ta plate (Fig. 3) is shown in Fig. 4.

The sound speed for Ta was measured to be 4230 ± 40 m/s, where the uncertainty in this case is associated with

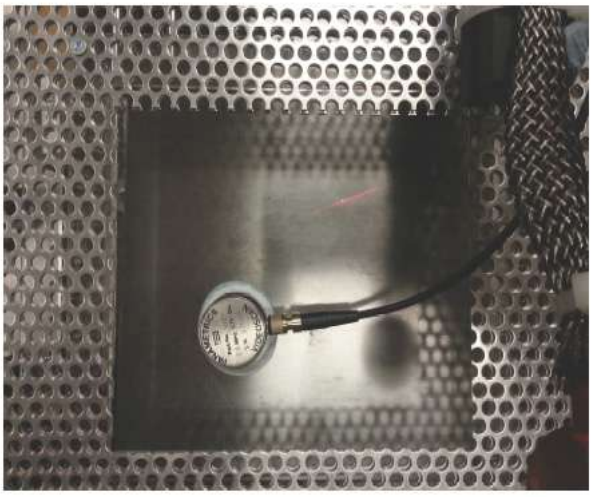

Figure 3. Ta plate 3 mm thick, 6"×6" transverse dimensions with a broadband transducer.

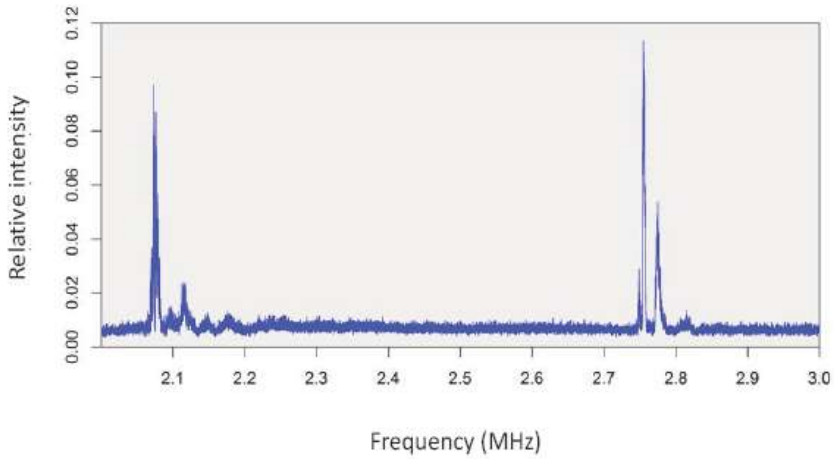

Figure 4. Compressional spectrum for the Ta plate of Fig. 3 near the $n = 3$ and $n = 4$ harmonics.

the plate thickness; this value is close to the 4100 m/s that can be found on tabulations. Note that loading by the relatively massive transducer causes mode splitting, corresponding to stronger vibrations at different locations on the plate surface.

3.2. Gel and water vibration

It was noticed that the ultrasound gel used to make contact between the transducer and the plate would seem to move during the frequency scans. The eye is not sufficiently fast to detect MHz motion, which means the gel would undergo a low frequency modification when the plate was driven near the fundamental. Subsequent experimentation with water (which was quickly lost) and with oil (which remained for a longer time) led to an ability to determine precise frequencies of maximum deformation which are produced at the fundamental.

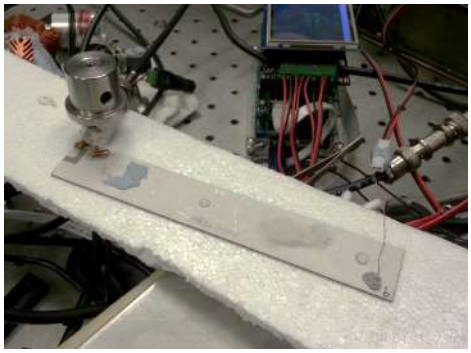

Figure 5. Piezoelectric transducer on Styrofoam.

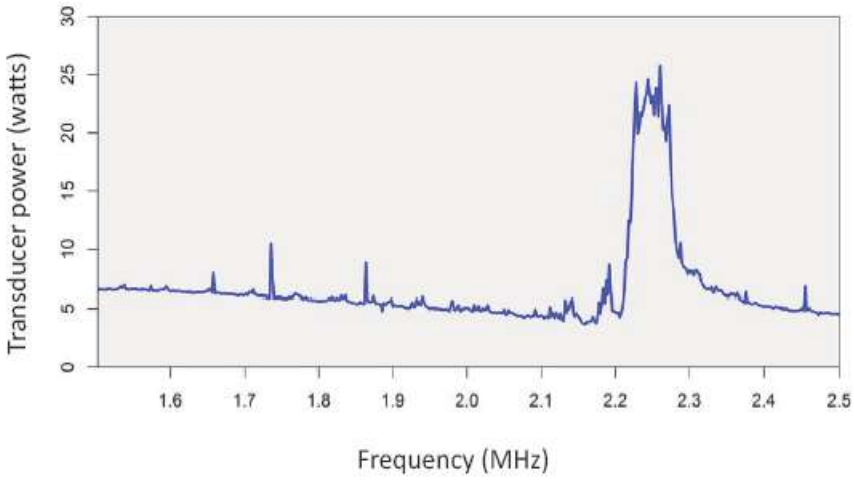

Figure 6. Transducer power spectrum (*black*) in the vicinity of its resonance on Styrofoam.

3.3. High-power piezo transducer

We obtained two high-power piezoelectric transducers with resonances near 2.23 MHz. One of the transducers on Styrofoam is shown in Fig. 5, with the transducer power spectrum (in isolation) shown in Fig. 6. The resonance of the piezo transducer is reasonably narrow, so in order to couple power between this transducer and a plate we need to work

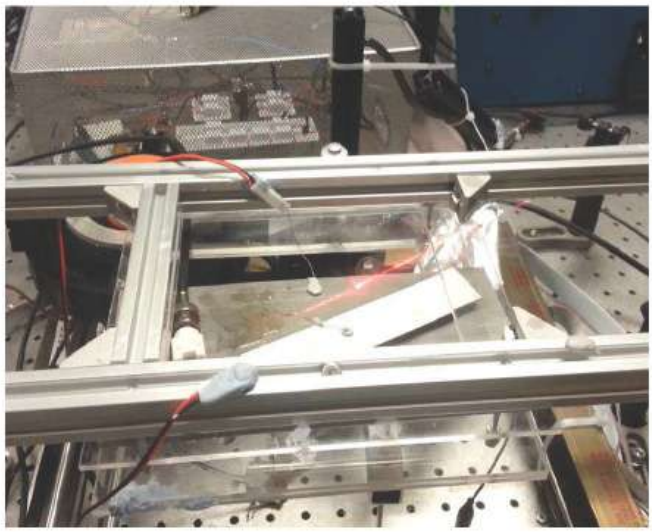

Figure 7. Piezoelectric transducer mounted on a matched steel plate.

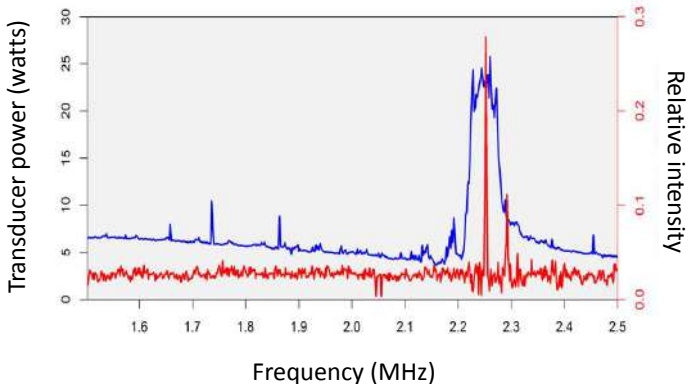

Figure 8. Transducer power spectrum (*black*) in the vicinity of its resonance on Styrofoam, and plate resonance (*red*).

with a plate with a matched resonance. This has been done by machining a thicker plate to the required thickness, and also by using plates ordered from a supplier that are made with thickness corresponding to a resonance. The resulting steel plate resonance is shown along with the transducer resonance in Fig. 7. We are able to drive the matched steel plate by placing the piezo transducer on the steel plate (Fig. 8) with an ultrasonic coupling gel between them.

3.4. Temperature measurements

We have been interested in how much vibrational energy is present (since up-conversion in the model depends on the level of vibrational excitation), and also in how much vibrational power is dissipated (since loss is important for up-conversion). The first thought was to use a Doppler measurement to determine the surface displacement, but we have as yet not managed to measure suitable Doppler signals for this purpose in the MHz regime. Additionally, the

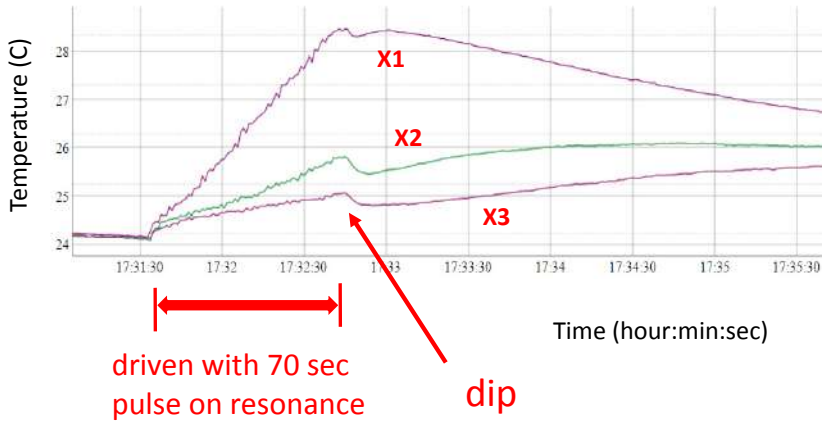

Figure 9. Transducer power spectrum on Styrofoam (*blue*) in the vicinity of the steel plate resonance (*red*).

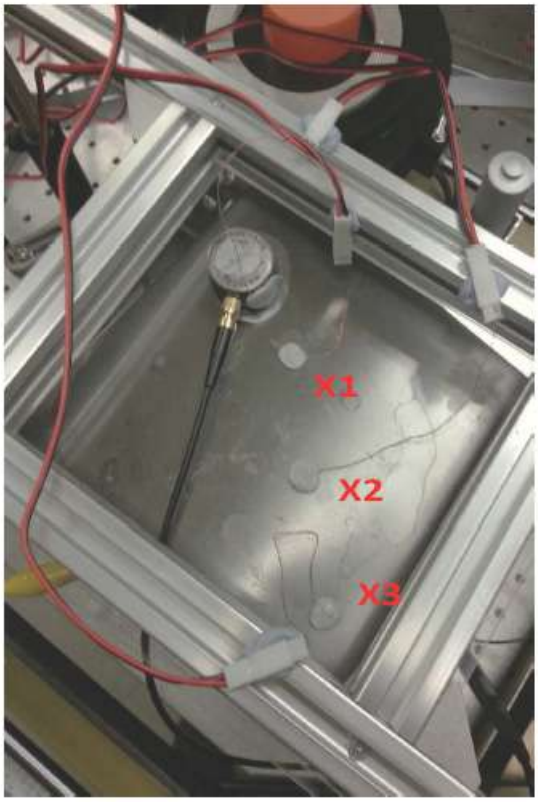

Figure 10. Plate driven on resonance at 2.1 MHz with thermal sensors.

displacement would have to be on the order of an optical wavelength to see sidebands, and it was not obvious at the time that we should expect such a large displacement based on the applied power.

Subsequently we noticed that the broad band transducers heated significantly, which we wanted to monitor to prevent overheating, and that the plates heated enough to be warm to the touch. Measurements of the plate temperature at different locations (Fig. 9) showed a slow temperature component that could be attributed to thermal conduction of heat from the transducer, and a fast component due to the dissipation of the vibrational energy. This effect was seen both when the transducer was turned on, and when turned off; a dip correlated with transducer turn off is illustrated in Fig. 10.

It was possible to develop an approximate calibration of the thermal response of the plate by putting in known thermal power from a resistive heater and measuring the temperatures. The thermal mass is substantial as can be seen in the linear temperature rise prior to the dip in Fig. 10. The incremental temperature in subsequent tests was fit to a single pole model

$$\left(\tau\frac{\mathrm{d}}{\mathrm{d}t}+1\right)\Delta T(t) \;=\; \left(\frac{\Delta T}{\Delta P}\right)P(t) \tag{5}$$

with a calibration constant $\Delta P/\Delta T$ of about 2.85 K/W and a time constant τ (due to the heat capacity) near 500 s. When the plate was driven on resonance with the high-power piezo transducer we observed a fast (delocalized) temperature increase of about 2.5°C with a 5-second long burst; according to the model this would correspond to about 100 W dissipated vibrational power in the harmonic. While we have found a simple single pole model adequate to allow an independent estimate of the vibrational power, a more sophisticated model would be required to account accurately for the position-dependent transport effects evident in the data shown in Fig. 10.

3.5. Ring-down measurement

Some attempts were made to determine the relaxation time of the vibrational energy making use of a ring-down measurement based on the amplitude modulation signal. Based on preliminary results the vibrations at 2.23 MHz probably decay with a time constant at or below 1.5 ms.

4. Experimental, Radiation Detection

In this section we describe some of the radiation detectors that we have worked with so far.

4.1. X-ray film, optical film, and light tight covers

Before this effort began, there was an exploratory attempt to measure X-rays from a steel plate in a Kornilova type of water-jet experiment, where X-ray film was used. In support of this experiment JET Energy Inc acquired a Kodak M35 X-OMAT processor to develop the X-ray film. Film from this exploratory experiment was processed and digitized using a Vidar VXR-16 Dosimetry Pro running RIT 113 Version 3.14 software.

X-ray film is exposed by visible light, and initially most films used were found to be exposed due to light leaks. Some following effort was devoted to debugging this and other issues, where optical film was used with light tight covering based on aluminum foil and with thin graphite sheets. Aluminum foil developed pinholes immediately, but the graphite was found to be somewhat less susceptible to pinholes. We were able to demonstrate direct X-ray exposure of optical film at an X-ray facility down to about 10 keV, with no obvious advantage from scintillators placed over the film. Preliminary experiments in the lab and at a waterjet were done with ISO 400 optical film (which we could develop in house), but no exposure that could be attributed to X-rays was seen.

4.2. Weak Fe-55 source and film

This motivated us to pursue X-ray diagnostics further in several directions. Subsequently we worked with a weak (15 μCi) Fe-55 source which allowed us to quantify the sensitivity of different detectors near 5.9 and 6.5 keV. With 1 and 2 day exposures of the source close to the film we could see a clear image, but only the faintest remnant was apparent on a light table after 1 h exposure (Fig. 11). It was found that optical film with higher ISO was much more sensitive. With ISO 1600 film we are able to see weak images from exposures as short as 10 min. As we have not yet succeeded in observing anomalous X-ray emission in any of our experiments so far, we have not yet returned to the use of X-ray film due to its lower sensitivity compared to other X-ray detection methods.

4.3. Scintillator with optical film and camera

Harder X-rays are imaged on film using planar scintillators, which is important since direct X-ray absorption by the film is reduced, and since the light produced increases with X-ray energy. We tried a number of different scintillators

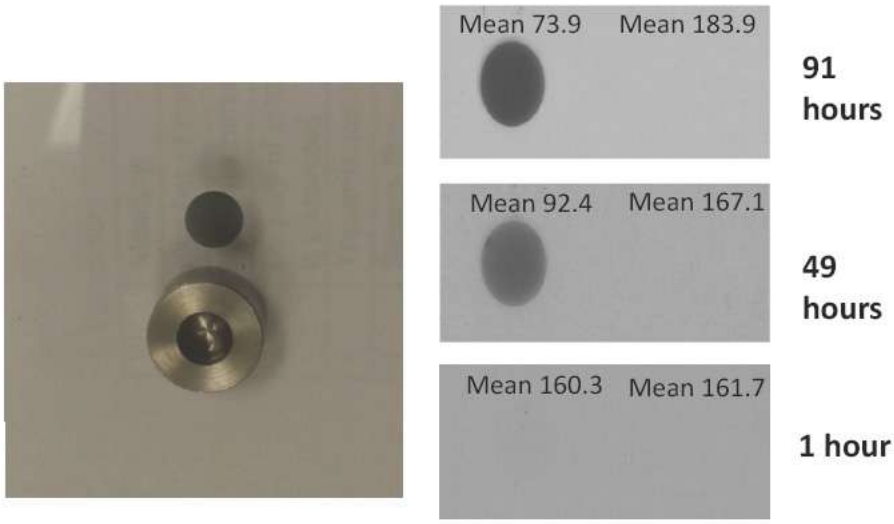

Figure 11. 15 μCi Fe-55 source and image produced on film (*left*); images on optical film for different exposures (*right*).

(Al-covered YAG:Ce, BC-400, BC-404, and ZnS), with some improvement above 10 keV, but no enhancement with the Fe-55 source compared with direct optical film exposure. We also tried experiments with scintillator and a sensitive camera normally used for astronomy in the hope of having real-time imaging, but the signals from the scintillator were weak compared to noise (Fig. 12).

Figure 12. Scintillator and camera (*left*); image from camera CCD for a strong Co-57 source above the scintillator (*right*).

Figure 13. ZnS scintillator/PMT X-ray detector.

4.4. Scintillator and PMT detectors

Since the CCD array of the camera was insensitive and noisy, and since the sensitivity of the film is marginal relative to more sensitive detectors, we were motivated to pursue X-ray detection based on a scintillator/PMT combination. It is possible to work with scintillators with high photon yield, even though there is some loss in the yield at low energy, and make use of the very good sensitivity of low cost photomultipliers to end up with a very sensitive X-ray detector. The X-ray is converted to many optical photons in the scintillator, some of which are detected by the PMT. An X-ray spectrum can be constructed following pulse shape analysis of the PMT output, which is normally done using sophisticated and moderately expensive pulse shape analyzer electronics. In recent years it has been recognized that much cheaper sound cards are capable of being used for this when the count rate is low, which has led to a new field of low cost gamma and X-ray detectors for students and hobbyists.

An X-ray detector was built by Florida-based iRad Inc, based on a 250 μ ZnS scintillator (normally used for alpha detection) and Hamamatsu 3" PMT (model R6233), with a thin radfilm cover (Fig. 13), with the analog signals read by a Focusrite 192 kHz low-noise USB audio interface and analyzed with open source Theremino MCA software. It is very much more sensitive than film: X-ray fluorescence from the Mn K-alpha ionized by Fe-55 sources is apparent in seconds. A minor drawback is that the resolution is poor; as can be seen in the Ti K-alpha spectrum at 4.5 keV shown in Fig. 14, which has a line width close to a keV. The absorption of the few microns of aluminum on the radfilm prevents us from seeing XRF K-alpha lines of silicon through calcium, but we have seen X-ray fluorescence from the Mg K-alpha at 1.25 keV.

A modified version of this detector with a Be window is being built, and we hope to test it in coming months. The scintillator is thin so that the detector is not sensitive to X-rays of more than about 20 keV. We have also acquired a similar detector with a 2" thick Saint Gobain BC-408 scintillator and Photonis 3" PMT (model XP5312) for gamma detection.

In addition, we have available an Amptek X-123 X-ray detector which has better energy resolution but poorer

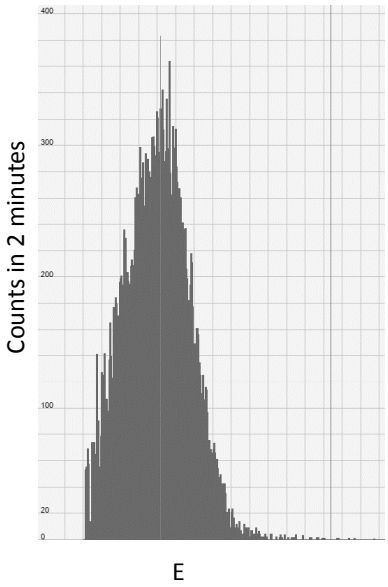

Figure 14. Two minute XRF spectrum of Ti K-alpha (4.5 keV) with background subtraction, from an X-ray fluorescence experiment with Fe-55 sources.

sensitivity than the scintillator/PMT detectors discussed above.

4.5. Neutron detection

We are also interested in the possibility of seeing whether neutron emission can be seen from vibrated steel samples, as has been claimed by Cardone and coworkers [10]. We have recently obtained a Wendi-2 He-3 neutron detector from Thermo Fisher, which has a listed sensitivity of 0.01 μSv/h. Data taken with this detector are shown in Fig. 15; we see a background count rate on the order of 0.2 cpm, which based on the 0.84 cps/μSv/h listed conversion is about 4 nSv/h. This is lower than a 0.45 cpm value measured outside, indicating some shielding by the building our lab is located in; and is also lower than the neutron background value of 14.5 nSv/h quoted in Ref. [16]. Motivated by the observations of Cardone and by Carpinteri, we have attempted a quick exploratory measurement looking for neutron emission from a steel plate vibrated with the piezo transducer at 2.23 MHz above 100 W (conditions very different than in the experiments mentioned above), with no counts obvious above background.

5. Experimental, Sample Preparation

We work with steel and copper plates from McMaster-Carr, and tantalum plates from Baoji Hanz Material Technology Co. Ltd. Some discussion is appropriate concerning the further processing of the samples.

5.1. Mercury on copper

We have conjectured that the 1565 eV transition in ^{201}Hg is responsible for collimated X-ray emission near 1.5 keV in the Karabut experiment [11], which due to the absence of absorption edges in the spectrum must be on or just below

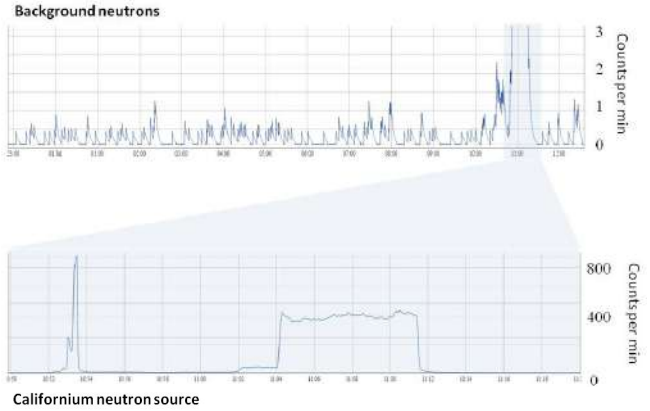

Figure 15. Laboratory background time history (*top*); elevated count rate with a Cf-252 neutron source (*bottom*).

the surface; the proposal is that it is present as a low-level contamination from the discharge. We might expect Hg to be present in our plates at low level as an uncontrolled impurity; however, since we have as yet no signals an obvious question can be raised as to whether we have sufficient Hg present to given us sufficient emission to detect. Hg binds strongly to copper, a fact exploited by Tanzella to plate a small amount of Hg onto the surface of copper foils for the tests at SRI [15]. We plan to make use of this approach to make available Cu foils with surface Hg that we can attach to a driven steel resonator, in the hope of clarifying whether this is how collimated X-rays are produced in the Karabut experiment.

5.2. Cobalt-57

In an excitation transfer experiment [17], a radioactive Co-57 source can produce excited state Fe-57 in the vicinity of the source; we will monitor for evidence that the excitation is transferred elsewhere in the plate. It is possible to acquire $^{57}CoCl_2$ in solution (from Eckert & Ziegler) and evaporate it on steel or other metal surfaces.

5.3. Tungsten-181

In a second version of the experiment radioactive W-181 can be generated in a localized region through $^{181}Ta(p,n)^{181}W$ reactions [18], and in this case we will monitor for signs that the 6.237 keV excited state has been induced away from the localized bombarded region.

6. Conclusion and Discussion

As discussed in the first two sections of the paper, a theoretical model with the potential for accounting systematically for many of the anomalies reported in our field has been developed over the past decades. According to this model there is a coupling between vibrations and internal nuclear degrees of freedom, and there is a mechanism that involves a highly excited oscillator coupled to many identical two-level systems that in the presence of loss predicts a strongly enhanced up-conversion and down-conversion effect. We would like to carry out experiments that would test these ideas. Excitation transfer requires the least in the way of new physics according to the models, and we are interested

in excitation transfer tests with Co-57 to produce excited states at 14.4 keV in Fe-57, and in W-181 to produce excited states at 6.2 keV in Ta-181. Up-conversion to produce excited states at 1.56 keV in Hg-201 is perhaps the next "easiest" goal. Up-conversion to produce gammas at higher energy is expected to be harder, and neutron emission from steel would probably be the "hardest" effect to produce in that it would require the most up-conversion of the experiment under consideration.

Up-conversion or down-conversion in the lossy spin–boson model is critically dependent on the presence of a strong loss effect. To date the majority of our experiments in the lab and with the waterjet have been done under conditions where the loss has been minimized; this can be understood in the context of the laboratory experiments in that we have been interested in maximizing the vibrational displacements in order to be able to see that we have succeeded in inducing vibrations and to be able to understand where the resonances are. An important issue in the experiments currently under consideration is to add loss, and to quantify the amount of loss present. For example, if we imagine that the nuclear energy in the two-laser experiment goes into THz vibrations, we know that such high frequency vibrational modes are very lossy, with a Q value on the general order of 10. If we interpret the collimated X-ray bursts in the Karabut experiment [6] as informing us as to the vibrational frequencies involved, then we might infer a frequency on the order of 10 kHz [19] and an associated time constant on the order of a few milliseconds. If so, then the Karabut experiment can be viewed as involving a low-Q and hence very lossy resonator.

Acknowledgements

We are grateful for equipment and advice provided by Dr. Mitchell Swartz and Dr. Alex Frank in the realm of X-ray diagnostics as well as for general feedback from Dr. Mitchell Swartz, Gayle Verner, and Jeff Tolleson during seminars and workshops. We would like to express appreciation to Industrial Heat for support in the form of unrestricted gift that we used for this work.

References

[1] M. Fleischmann and S. Pons, Electrochemically induced nuclear fusion of deuterium, *J. Electroanal. Chem. Interfacial Electrochem.* **261** (1989) 301–308.

[2] M. Fleischmann, S. Pons, M. W. Anderson, L. J. Li and M. Hawkins, Calorimetry of the palladium-deuterium-heavy water system, *J. Electroanal. Chem. Interfacial Electrochem.* **287** (1990) 293–348.

[3] E Storms, *The Science of Low Energy Nuclear Reaction: A Comprehensive Compilation of Evidence and Explanations about Cold Fusion*, World Scientific, Singapore, 2007.

[4] P.L. Hagelstein, Current status of the theory and modeling effort based on fractionation, *J. Condensed Matter Nucl. Sci.* **19** (2016) 98–109.

[5] P.L. Hagelstein, Quantum composites: A review, and new results for models for Condensed Matter Nuclear Science, *J. Condensed Matter Nucl. Sci.* **20** (2016) 139–225.

[6] A.B. Karabut, E.A. Karabut and P.L. Hagelstein, Spectral and temporal characteristics of X-ray emission from metal electrodes in a high-current glow discharge, *J. Condensed Matter Nucl. Sci.* **6** (2012) 217–240.

[7] A.A. Kornilova, V.I. Vysotskii, N.N. Sysoev, N.K. Litvin, V.I. Tomak and A.A. Barzov, Generation of intense X-rays during ejection of a fast water jet from a metal channel to atmosphere, *J. Surface Investigation: X-ray, Synchrotron and Neutron Techniques* **4** (2010) 1008–1017.

[8] F. Cardone, G. Cherubini, M. Lammardo, R. Mignani, A. Petrucci, A. Rosada, V. Sala, and E. Santoro, Violation of local Lorentz invariance for deformed space–time neutron emission, *Eur. Phys. J. Plus* **130** (2015) 55.

[9] A. Carpinteri, G. Lacidogna, A. Manuello and O. Boria, Piezonuclear fission reactions from earthquakes and brittle rocks failure: evidence of neutron emission and non-radioactive product elements, *Exp. Mech.* **53** (2013) 345–365.

[10] P.L. Hagelstein and I.U. Chaudhary, Coherent energy exchange in the strong coupling limit of the lossy spin–boson model, *J. Condensed Matter Nucl. Sci.* **5** (2011) 116–139.

[11] P.L. Hagelstein, Bird's eye view of phonon models for excess heat in the Fleischmann–Pons experiment, *J. Condensed Matter Nucl. Sci.* **6** (2012) 169–180.
[12] P.L. Hagelstein and I.U. Chaudhary, Models for phonon–nuclear interactions and collimated X-ray emission in the Karabut experiment, *J. Condensed Matter Nucl. Sci.* **13** (2014) 177–222.
[13] P.L. Hagelstein and I.U. Chaudhary, Anomalies in fracture experiments, and energy exchange between vibrations and nuclei, *Meccanica* **50** (2015) 1189–1203.
[14] F. Cardone, G. Albertini, D. Bassani, G. Cherubini, E. Guerriero, R. Mignani, M. Monti, A. Petrucci, F. Ridolfi, A. Rosada and F. Rosetto, Nuclear metamorphosis in mercury, *Int. J. Modern Phys. B* **30** (2016) 1550239.
[15] F. Tanzella, J. Bao, M.C.H. McKubre and P.L. Hagelstein, Seeking X-rays and charge emission from a copper foil driven at MHz frequencies, *J. Condensed Matter Nucl. Sci.* **19** (2016) 110–118.
[16] M. Brugger, P. Carbonez, F. Pozzi, M. Silari and H. Vincke, New radiation protection calibration facility at CERN, *Radiation Protection Dosimetry* **161** (2013) 181–184.
[17] P.L. Hagelstein and I.U. Chaudhary, Coupling between the center of mass and relative degrees of freedom in a relativistic quantum composite and applications, *J. Condensed Matter Nucl. Sci.* **24** (2017).
[18] V.A. Dornow, J. Binder, A. Heidemann, G.M. Kalvius and G. Wortmann, Preparation of narrow-line sources for the 6.2 keV Mössbauer resonance of ^{181}Ta, *Nucl. Instr. Methods* **163** (1979) 491–497.
[19] P.L. Hagelstein, Probabilistic models for beam, spot, and line emission for collimated X-ray emission in the Karabut experiment, *J. Condensed Matter Nucl. Sci.* **22** (2017) 53–73.